HHS Public Access

Author manuscript

Nat Genet. Author manuscript; available in PMC 2018 December 28.

Published in final edited form as:

Nat Genet. 2018 April ; 50(4): 515–523. doi:10.1038/s41588-018-0044-9.

Enhancer invasion shapes MYCN dependent transcriptional amplification in neuroblastoma

Rhamy Zeid[1], **Matthew A. Lawlor**[1], **Evon Poon**[2,3], **Jaime M. Reyes**[1], **Mariateresa Fulciniti**[1,4], **Michael A. Lopez**[1,4], **Thomas G. Scott**[1], **Behnam Nabet**[1], **Michael A. Erb**[1], **Georg E. Winter**[1], **Zoe Jacobson**[1], **Donald R. Polaski**[1], **Kristen L. Karlin**[5], **Rachel A. Hirsch**[5], **Nikhil P. Munshi**[1,4], **Thomas F. Westbrook**[5], **Louis Chesler**[2,3], **Charles Y. Lin**[1,5], and **James E. Bradner**[1,6,7]

[1]Dana-Farber Cancer Institute, Department of Medical Oncology, Boston, MA.

[2]Divisions of Clinical Studies, The Institute of Cancer Research, London, UK.

[3]Cancer Therapeutics, The Institute of Cancer Research, London, UK.

[4]LeBow Institute for Myeloma Therapeutics and Jerome Lipper Multiple Myeloma Center, Dana-Farber Cancer Institute, Boston, MA.

[5]Baylor College of Medicine, Department of Molecular and Human Genetics, Houston, TX.

[6]Department of Medicine, Harvard Medical School, Boston, MA.

[7]Novartis Institute for Biomedical Research, Cambridge, MA.

Abstract

Amplification of the oncogenic transcription factor MYCN is a defining genetic feature of high-risk neuroblastoma. Here, we present the first dynamic chromatin and transcriptional landscape of

Correspondence: Charles Y. Lin, Charles.y.lin@bcm.edu, James E. Bradner, James.bradner@novartis.com. *Co-corresponding authors.

Author Contributions

R.Z., C.Y.L and J.E.B. designed this study. R.Z. designed and performed biology experiments. C.Y.L, J.M.R., D.R.P, and R.A.H. performed data analysis. M.A. Lawlor assisted in ChIP-seq experiments. E.P. performed mouse experiments. M.F. and M.A. Lopez. performed experiments in multiple myeloma. T.G.S, Z.J., and K.L.K assisted in cellular assays. B.N. assisted in RNA-seq profiling. M.A.E and G.E.W assisted in exon-scanning CRISPR-Cas9. N.P.M, T.F.W and L.C. supervised experiments. R.Z., C.Y.L., and J.E.B. analyzed results and wrote the manuscript with comments from all authors.

Competing Financial Interests

R.Z. is now an employee of C4 Therapeutics. C.Y.L. is a consultant of Jnana Therapeutics and is an shareholder and inventor of IP licensed to Syros Pharmaceuticals. J.E.B. is a Scientific Founder of Syros Pharmaceuticals, SHAPE Pharmaceuticals, Acetylon Pharmaceuticals, Tensha Therapeutics (now Roche) and C4 Therapeutics and is the inventor on IP licensed to these entities. J.E.B. is now an executive and shareholder in Novartis AG. Correspondence and requests for materials should be addressed to Charles Y. Lin (charles.y.lin@bcm.edu) or James E. Bradner (james.bradner@novartis.com)

Additional methods are provided in the **Supplementary Note**.

URLs

R package survival and KM plotting script: http://statbandit.wordpress.com/2011/03/08/an-enhanced-kaplan-meier-plot/).
Bamliquidator (version 1.0) read density calculator: https://github.com/BradnerLab/pipeline/wiki/bamliquidator.
ENCODE blacklist: https://sites.google.com/site/anshulkundaje/projects/blacklists
ROSE2 software package: https://github.com/BradnerLab/pipeline-ROSE2_main.py

Data availability

All ChIP-seq, RNA-seq, ATAC-seq, and microarray data generated in this publication can be found online associated with GEO Publication Reference ID GSE80154. GEO accession numbers and respective details for all analyzed datasets can also be found in supplemental tables (Supplementary Table 6-8).

MYCN perturbation in neuroblastoma. At oncogenic levels, MYCN associates with E-box binding motifs in an affinity dependent manner, binding to strong canonical E-boxes at promoters and invading abundant clustered weaker non-canonical E-boxes at enhancers. Loss of MYCN leads to a global reduction in transcription. However, the most highly enhancer occupied MYCN target genes are more sensitive to MYCN perturbation, tissue specific, and associated with poor patient survival. Activity of MYCN enhancer occupied genes is dependent on the tissue-specific transcription factor TWIST1 which co-occupies enhancers with MYCN and is required for MYCN dependent proliferation. These data implicate tissue-specific enhancers in predicating often highly tumor specific “Myc target gene signatures” and identify disruption of the MYCN enhancer regulatory axis as a promising therapeutic strategy in neuroblastoma.

Introduction

The Myc family of transcription factors (TFs), comprised of *MYC*, *MYCN*, and *MYCL*, are together the most commonly altered oncogenes in cancer[1, 2]. They normally function as master integrators of cellular growth signals and mediate a transcriptional response involved in a variety of processes including proliferation, cell growth, differentiation, survival, and pluripotency. The *MYCN* oncogene is a characteristic feature of aggressive, relapsed neuroblastoma, an aggressive pediatric cancer arising from neural crest tissue[3, 4]. Targeted MYCN overexpression in peripheral neural crest is sufficient to initiate disease in mouse models[5]. MYCN down-regulation broadly reverses tumor stem-like phenotypes[6, 7] and aberrant proliferation[8-11] in a variety of neuroblastoma models[12-14], and recent therapeutic strategies to indirectly target MYCN production or protein stability have reduced tumor growth *in vivo*[15-17].

Whereas MYCN function has not been dynamically characterized using incisive genome-wide measurements, several recent studies have considered the transcriptional consequences of elevated MYC levels, presenting two seemingly conflicting views on the mechanistic consequence of MYC deregulation in cancer[18-21]. First, MYC has been reported to function in a context-specific manner, activating or even repressing discrete target genes[20, 21]. Alternatively, MYC has been found to broadly remodel the cancer *cis*-regulatory landscape leading to increased transcription at all active genes promoting global transcriptional amplification[18, 19]. At physiological levels, both models predict MYC binding to high affinity canonical (CACGTG) E-box sites at the promoters of genes involved in growth and proliferation. At deregulated levels, highly abundant MYC proteins, which can only bind to regions of open and accessible chromatin, saturate the cell’s active *cis*-regulatory landscape, binding to prevalent degenerate non-canonical CANNTG E-boxes to effect a complex systemic and pleiotropic transcriptional consequence[22]. This is further complicated by the numerous functional roles of MYC family proteins, their complex interaction networks, and the difficulty in discriminating direct effects of MYC binding from secondary indirect consequences[21]. These observations suggest that MYC blurs the line between a gene-specific and global gene control factor, with a small number of genes uniquely evolved to rapidly respond to perturbations in MYC levels and other functional responses largely predicated on the cell’s pre-established chromatin landscape and gene expression program[23].

To understand the functional consequence of MYCN activation, and to resolve residual ambiguity regarding Myc-family TF mechanisms of genome-wide transcriptional regulation, we performed kinetic studies of MYCN activation and withdrawal in neuroblastoma.

Results

Deregulated MYCN binds active chromatin and amplifies transcription in neuroblastoma

To first profile MYCN downregulation from oncogenic levels, we experimentally selected a panel of human neuroblastoma cell lines with and without *MYCN* amplification that express varying levels of MYCN (Fig. 1a; Supplementary Fig.1a), and employed the well-characterized *tet*-off MYCN SHEP-21N cell line model[24] (Fig. 1b; Supplementary Fig. 1b and Supplementary Table 1). Additionally, we explored the consequences of MYCN induction by engineering a *tet*-on MYCN model in the parental SHEP neuroblastoma cell line grown for multiple passages in a low MYCN state (Fig. 1c). Across MYCN-amplified neuroblastoma lines, we used chromatin immunoprecipitation coupled to high-throughput sequencing (ChIP-seq) to generate a consensus genome-wide map of ~10,000 regions that exhibit strong and consistent MYCN occupancy (Supplementary Fig. 1c; supplemental methods).

In a deregulated state, MYC binds to virtually all active promoters and subsequently 'invades' promoter-distal enhancer regions[18, 19, 21]. Comparably, we identify deregulated MYCN at active promoters e.g. at *NPM1* (Fig. 1d) that are corroborated by the presence of active transcription marks/factors (H3K4me3, BRD4, RNA Pol II) in BE(2)-C. Genome-wide conserved MYCN binding regions occur almost exclusively (96%) at active promoters and enhancers and show a strong concordance with active chromatin acetylation (H3K27ac), with virtually no overlap with regions of repressive H3K27me3 (Fig. 1e; Supplementary Fig. 1d-i; supplemental methods)

We next aimed to characterize the hierarchy of binding at active promoters and enhancers. We find that MYCN signal correlates with H3K27ac signal and these regions of increased binding overlap more with active TSS regions versus distal enhancers (Supplementary Fig. 1j). Trends in MYCN loading are reflected in the underlying sequence composition of binding sites. Strong promoter associated sites are highly enriched for the canonical (CACGTG) E-Box whereas weaker sites found at promoters and distal enhancers show higher enrichment of clustered non-canonical (CANNTG) E-boxes (Fig. 1e; Supplementary Fig. 1j). These trends in E-box occupancy are re-capitulated by *de novo* motif finding at promoters and enhancers (Fig. 1e) and are consistent with MYCN broadly associating with active regulatory elements in an affinity dependent manner, as previously observed for MYC[19, 25]. These data support a model that when deregulated, MYCN binds strongly at canonical E-boxes found at promoters of active genes (e.g. *RPL22*) and at clustered non-canonical E-boxes found at weaker promoters and distal enhancers (e.g. *ID2*), (Supplementary Fig. 1d,e).

We next investigated the dynamic chromatin and transcriptional consequences of direct MYCN depletion. Using the controllable *tet*-off MYCN SHEP-21N cells, we rapidly and synchronously eliminated MYCN with a 96% reduction achieved after only six hours (Fig.

1b). Distinct from prior studies of MYC inactivation, we characterized rapid kinetic effects of dynamic modulation of MYCN (0, 2, and 24 hours post inactivation) to profile changes in a high, medium, and low MYCN state. In anticipation of global changes to chromatin and transcription that might be masked by relative chromatin enrichment methods, we complemented traditional ChIP-seq methods with the cell count normalized ChIP-Rx[26] approach to quantify absolute changes in MYCN, H3K27ac, H3K4me3, CTCF, and RNA Poll II occupancy (Supplementary Fig. 2a,b; supplemental methods).

We observe that two hours after shutdown, MYCN is significantly depleted from promoters and enhancers (Fig. 1f; Supplementary Fig. 2c,e,f) — a result revealed by ChIP-Rx cell-count normalization (Supplementary Fig. 2e,f). At the exemplary MYC target gene *NPM1*, loss of MYCN from promoter regions initially results in a decrease of elongating RNA Pol II and subsequent loss of *NPM1* mRNA, suggesting that MYCN directly promotes transcription elongation, again akin to MYC (Fig. 1d,h). Overall early defects in transcriptional pause release culminate in loss of active chromatin marks and both initiating and elongating RNA Pol II, resulting in a global dampening of mRNA steady state levels (Fig.1g-i>; Supplementary Fig. 2d-j). Although both traditional ChIP-seq and ChIP-Rx reveal global loss of MYCN at promoters and enhancers, we do observe global loss of additional marks (H3K4me3, CTCF, H3K27ac, and RNA Pol II) at 24 hours post MYCN shutdown only in ChIP-Rx data (Supplementary Fig. 2g, Supplementary Fig. 3a-c). As all ChIP-Rx datasets show this global effect, in the absence of a negative control, we hypothesize, but cannot conclude with certainty that MYCN shutdown has global effects on chromatin compaction in neuroblastoma, as has been recently reported for MYC in B cell activation[27]. We do note that by global H3K27ac quantification, we observe a global loss in chromatin acetylation 24 hours after MYCN shutdown (Supplementary Fig. 2h), an observation also consistent with previous reports that MYC regulates global chromatin accessibility. In contrast, induction of MYCN in parental SHEP neuroblastoma cells (Fig. 1c,d) results in loading of MYCN at active promoters and enhancers, and is coincident with increases in global H3K27ac (Supplementary Fig. 3d-f). These data are consistent with MYCN acting as a global amplifier of transcription in neuroblastoma.

Enhancer invasion shapes MYCN transcriptional response in neuroblastoma

To better assess the direct contribution of MYCN to transcriptional response at individual genes, we hypothesized a direct relationship between underlying MYCN sequence affinity at promoter/enhancer regions, MYCN loading at these regions, and the resulting transcriptional response upon MYCN perturbation (Fig. 2a). Visual inspection of MYCN load at highly occupied genes revealed a diversity of binding profiles with some genes exhibiting promoter MYCN binding (*RPL22*) and others a more mixed array of promoter and enhancer binding (*HAND2 & ID2*) (Fig. 2b).

As enhancers are highly tissue specific and context dependent, we sought to determine whether similar MYCN enhancer invasion occurred *in vivo*. Profiling of the TH-MYCN genetically engineered neuroblastoma mouse model[28] (Supplementary Fig. 4a) revealed MYCN binding at the promoters of classic MYC target genes (*Npm1*/*Rpl22*), as well as at enhancers for key neuroblastoma and/or neural crest associated genes (*ID2* and *GATA2*)

(Fig. 2c; Supplementary Fig. 4b,c). Notably, MYCN binding also occurs at additional enhancers that others have shown to be lineage or tumor specific[29], such as the *Mirlet7b* and *Lin28* loci respectively (Supplementary Fig. 4d,e). Let-7 is a prominent miRNA tumor suppressor that is often post-transcriptionally attenuated by induction of Lin28 in neuroblastoma[29]. Overall, 69% and 36% of conserved neuroblastoma MYCN bound promoters and enhancers in human cell lines exhibited evidence of chromatin acetylation (H3K27ac) in TH-MYCN tumors and/or the celiac and superior cervical ganglia, the established tumor tissues of origin that display little MYCN activity (Supplementary Fig. 4a,f). Together, these data suggest that deregulated MYCN binds to and invades developmental enhancers that are pre-established. In support of this hypothesis, induced MYCN in SHEP parental cells (cultivated over time without MYCN) overwhelmingly binds to and invades pre-acetylated promoters and enhancers (Fig. 2d; Supplementary Fig. 3a,b).

Globally, genes with the highest total MYCN signal at proximal regulatory loci (i.e. promoter + and nearby <50kb distal enhancer MYCN) exhibited the highest levels of MYCN enhancer occupancy and relative fraction of enhancer MYCN contribution (Fig. 2e). This enhancer MYCN loading occurred at broad regions of enhancer occupancy with high overall levels of MYCN, suggesting that distal enhancers provide a reservoir for excess MYCN that is only accessed upon deregulation. This is observed both for MYCN in SHEP21-N cells and as well averaged across neuroblastoma cell lines (Supplementary Fig. 5a,b). Indeed, 2 and 24 hours after MYCN shutdown, weaker MYCN binding sites at enhancers are preferentially depleted in SHEP21-N cells when compared to canonical E-box enriched promoter sites. Conversely, induction of MYCN results in the opposite effect, with promoter sites preferentially gaining MYCN binding sites (Fig. 2f, Supplementary Fig. 3d). Preferential enhancer loss corresponds to increased transcriptional sensitivity as measured using both cell count normalized and relative profiling of mRNA levels and elongating RNA Pol II density (Fig. 2g,h; Supplementary Fig. 5c-f). These findings are recapitulated in BE(2)-C cells by JQ1, a BET bromodomain inhibitor that we have previously shown to selectively deplete MYCN in neuroblastoma (Supplementary Fig. 6)[17]. Overall, we observe a strong dose dependence between MYCN signal and transcriptional response suggesting that MYCN affinity of underlying promoter and enhancer regions shapes MYCN dependent transcriptional amplification in neuroblastoma. Importantly, the top 25 highly loaded and MYCN sensitive genes can accurately stratify neuroblastoma overall survival in all patients and specifically in patients without evident MYCN amplification, a cohort that is generally considered low risk[30] (Fig. 2i and Supplementary Table 2).

Enhancer invasion accounts for tumor specific MYC/MYCN signatures

Cellular processes and developmental transitions are regulated by cell type specific enhancers. The observed enhancer invasion by deregulated MYCN suggests that MYC family transcription factors may act through pre-established enhancers to amplify tissue-specific gene expression[31, 32]. Toward a general explanation, we investigated active enhancer landscapes in the context of both MYCN (neuroblastoma) and MYC (four tumor types) deregulation. We first examined enhancer structure and MYC/MYCN occupancy at canonical tissue-specific genes. In neuroblastoma cell lines, we observe neuroblastoma specific enhancer activity and coinciding MYCN binding at the enhancer for tyrosine

hydroxylase (TH), a neural crest lineage marker[28], while we observe multiple myeloma specific enhancer activity and coinciding MYC binding at the enhancer for the plasma lineage factor IRF4[33]. Lastly, at the promoter dominant gene NPM1 we observe conserved MYC/MYCN binding, which is active in both tumor types (Fig. 3a).

To test this hypothesis globally, we ranked the top 5,000 MYCN loaded genes by their relative promoter/distal enhancer MYCN contribution and performed leading edge functional analysis (Fig 3b-e). We find that promoter dominant genes statistically enriched for the classically defined core MYC target gene set[34-39], whereas distal enhancer dominant genes included key neuroblastoma oncogenes (HAND2 & ID family TFs) and neural crest markers (TH), and were enriched for known signaling signatures in neuroblastoma including response to Tretinoin (retinoic acid), a pro-differentiating agent used clinically to treat high-risk neuroblastoma[40]. Similar analysis comparing MYCN to the enhancer mark H3K27ac in BE(2)-C cells produced distinct promoter/distal enhancer signatures (Supplementary Fig. 7a-h,k), suggesting a MYCN specific pattern of enrichment. Notably, genes on both the promoter dominant and enhancer dominant leading edge were capable of stratifying neuroblastoma patient overall survival suggesting that both promoter and enhancer dominant genes contain important oncogenic gene expression programs (Supplementary Fig. 7i,j and Supplementary Table 2).

Importantly, shutdown of MYCN preferentially depleted distal enhancer gene signatures, whereas induction of MYCN first established promoter gene signatures prior to distal enhancer signatures (Fig. 3f; Supplementary Fig. 7l). These data suggest that deregulated MYCN invades enhancers to drive tumor specific processes in neuroblastoma.

When this same analysis was performed with 4 additional models of MYC driven cancers (*MYC* amplified small cell lung cancer, *IgH/MYC* translocated multiple myeloma, Burkitt lymphoma, and glioblastoma), we again resolved increased enhancer contribution at highly occupied genes (Supplementary Fig. 8). Consistent with the tissue/tumor specific nature of enhancers, we observed much stronger correlation of MYC promoter binding relative to enhancers (Fig. 3g,h). Distal enhancer/promoter analysis revealed the MYC core target gene set and associated housekeeping gene signatures at the promoter dominant leading edge conserved across tumors. However, in contrast to neuroblastoma, distal enhancer dominant MYC bound genes enriched for their respective tumor-specific pathways including chr16p13 amplification in small cell lung cancer[41], chemokine and CD40 signaling in multiple myeloma[42-45], Epstein-Barr Virus in multiple myeloma and Burkitt lymphoma[46], and FOXO3 targets in glioblastoma[47]. Notably chromatin pathways appeared as a MYC/MYCN enhancer regulated signature in multiple tumors contexts[48, 49] (Fig. 3i). These data suggest that enhancer invasion can account for the divergent and often puzzling consequences of oncogenic MYC/MYCN activation and provide a rationale for the tumor specific oncogenic phenotypes observed upon MYC/MYCN deregulation.

TWIST1 co-occupies enhancers with MYCN and is required for expression of the MYCN enhancer axis

If MYCN enhancer invasion accounts for the tumor specific consequences of MYCN deregulation, then the TFs that establish tissue specific enhancers likely define MYCN

enhancer responsive gene expression programs. In any given cell type, a small set of tissue specific TFs are regulated by large clusters of enhancers (so-called super-enhancers or SEs), and these SE-associated TFs themselves often occupy the vast majority of active enhancers and super-enhancers as a core regulatory circuit[50, 51]. Thus, an integrated computational analysis of TF motif occupancy at SEs may allow the inference of TFs that define enhancer landscapes. We applied a recently reported methodology developed by our lab to define the highly-interconnected core regulatory circuitry of enhancer regulating TFs[52, 53] (Supplementary Fig. 9a-d). The consensus circuitry includes several well established regulators of neuroblastoma identity including MEIS1/2, GATA2/3, PHOX2A/B and HAND2[54-56] that are not present in other unrelated tumor circuitries (Supplementary Fig. 10). These data are consistent with recently reported studies identifying at least two distinct cell states as defined by core regulatory circuitries including an adrenergic/sympathetic noradrenergic and a mesenchymal/neural crest cell state[57, 58]. Specifically, we find that cell lines BE(2)-C, NGP, and Kelly correspond to the adrenergic/sympathetic noradrenergic state characterized by PHOX2B, PHOX2A, and GATA3 (Supplementary Fig. 9b-c). SHEP-21N which was derived from the parental SHEP line corresponds to the mesenchymal/neural crest cell state and is defined by PRRX1 and members of the AP-1 TF family (Supplementary Fig. 9b-c). From this analysis, we also retrieve the TFs TWIST1 and HAND2 across cell lines of both states which are lineage specific bHLH TFs with a well-established role in promoting tumorigenesis in several human cancers including neuroblastoma[59-61] (Supplementary Fig. 9d).

Since bHLH TFs recognize E-box CANNTG motifs, we hypothesized that the clustered non-canonical E-boxes at enhancers invaded by MYCN might be proximally occupied by TWIST1 and HAND2, and that these factors may collaborate to drive oncogenic enhancer transcription. Indeed, high affinity TWIST1 and HAND2 sites are predicted at > 80% of all MYCN enhancer sites (Fig. 4a). As TWIST1 has been implicated in MYCN amplified neuroblastoma[62], we sought to investigate its role and relation to MYCN in regulating neuroblastoma enhancer driven transcription. Performing ChIP-seq for TWIST1 in the SHEP-21N and BE(2)-C lines, we observe strong overlap of MYCN and TWIST1 at enhancers and show by *de novo* motif finding that TWIST1 recognizes a CANNTG E-box similar to enhancer bound MYCN (Fig. 4b-c). Inspection of individual MYCN invaded enhancer loci reveal spatially proximal co-localization of MYCN/TWIST1 at clustered non-canonical E-box motifs (Fig. 4d). Unexpectedly, MYCN shutdown broadly depletes genomic bound TWIST1 at 24 hours with minimal change in TWIST1 protein levels (Fig. 4e,f), suggesting an important regulatory link that is further emphasized by the correlative relationship between MYCN loss and TWIST1 at MYCN/TWIST1 co-occupied regions (Supplementary Fig. 9e). Overall, genes with proximal and strong MYCN/TWIST1 occupied enhancers are more potently down-regulated by MYCN shutdown than genes associated with strong MYCN only (Fig. 4g). Finally, these high MYCN/TWIST1 occupied genes also stratify patient overall survival (Fig. 4h and Supplementary Table 2), implicating the MYCN/TWIST1 regulated gene expression program in neuroblastoma.

As a regulator of mesenchymal lineage and de-differentiated cell state in tumors, TWIST1 specifies target genes, but relies on other cues, including potentially MYCN, to enforce transcriptional activation or repression. To evaluate TWIST1 as a deregulated MYCN-

specific neuroblastoma dependency, we utilized CRISPR Cas9, siRNA, and shRNA genetic approaches to perturb TWIST1. First, CRISPR Cas9 mutagenesis scanning of the TWIST1 locus and its large proximal enhancers with a multiplexed library of 3,351 single guide RNAs (sgRNAs) revealed TWIST1 *cis*-regulatory enhancer elements as required for neuroblastoma proliferation (Fig. 4i,j and Supplementary Table 3) — a result not seen with similar CRISPR Cas9 scanning of the expressed chromatin regulator NSD1 (Supplementary Fig. 9f,g and Supplementary Table 4). These data provide initial validation for the essentiality of *cis*-regulatory enhancers participating in the predicted neuroblastoma core regulatory circuitry. Second, siRNA depletion of TWIST1 revealed a MYCN dependent effect in neuroblastoma as seen across cell lines with high (BE(2)-C) vs. low (SH-SY5Y) MYCN, and in the isogenic SHEP21-N system at high and low MYCN states (Supplementary Fig. 9h,i and Supplementary Table 4). Finally, induced shRNA mediated kinetic TWIST1 knockdown reduces neuroblastoma proliferation in BE(2)-C cells (Fig. 4k and Supplementary Table 3) and selectively down-regulates only genes with high MYCN enhancer signal and fails to preferentially down-regulate high MYCN promoter loaded genes (Fig. 4l). This observation is in contrast to MYCN shutdown which preferentially down-regulates genes ranked either by promoter or enhancer MYCN signal (Supplementary Fig. 9j). These data establish TWIST1 as a key regulator of the MYCN enhancer axis and suggest a potent oncogenic collaboration between TWIST1/MYCN in driving enhancer dependent neuroblastoma gene expression.

Discussion

When deregulated, MYCN dominates the active *cis*-regulatory landscape of neuroblastoma to enforce both proliferation through promoter binding and de-differentiation through enhancer invasion. We establish that MYCN load at promoters and proximal enhancers predicts transcriptional responsiveness to MYCN shutdown and that MYCN enhancer binding occurs prominently at the most strongly occupied and down-regulated genes, suggesting a role for these tissue specific elements in predicating MYCN responsive “target” genes.

In neuroblastoma, oncogenic collaboration of MYCN and TWIST1 at enhancers demarcates a set of developmental genes important to neuroblastoma tumorigenesis and highly sensitive to both MYCN and TWIST1 perturbation. In contrast, in the B-cell malignancies multiple myeloma and Burkitt lymphoma that do not express HAND or TWIST factors, we instead identify and validate TCF3 (E2A) as a bHLH TF that is selectively required for growth of MYC deregulated multiple myeloma, and may play an equivalent role as TWIST1 (Supplementary Fig. 10 and Supplementary Table 5). These data demonstrate the extensibility of an approach to identify unrecognized tumor dependencies among core regulatory TFs, via collaborative gene control with Myc family oncoproteins.

Finally, instead of focusing only on the overall global transcriptional consequences of MYCN shutdown, or more narrowly at the most differentially regulated target genes, our results prompt a more quantitative consideration of MYCN as a dose dependent amplifier of transcription that is shaped by E-box rich *cis*-regulatory elements at promoters and enhancers. Whereas highly MYC/MYCN bound promoters are active in a majority of cell

types, the enhancer dominant MYC/MYCN bound genes vary greatly between tumor types, suggesting that enhancers and the factors that form them are responsible for imparting gene selectivity and producing the often divergent and tumor specific MYC/MYCN responses[63]. Notably, highly MYCN loaded genes stratify patient overall survival, an effect that is improved by incorporating the MYCN enhancer axis. Interestingly, this gene set is able to stratify patients without genomic *MYCN* amplification, a cohort with typically favored prognosis for which there are few means to reliably identify high risk individuals. Additionally, these data suggest that certain neuroblastoma tumors without MYCN deregulation are able to activate this oncogenic gene expression program. These data provide the first molecular characterization of the direct MYCN occupied gene expression program and its role in patient disease progression.

Online Methods

Cell lines.

SK-N-AS, SH-SY5Y, NGP, BE(2)-C, and KELLY cells were kindly provided by Dr. Kimberly Stegmaier (Dana Farber Cancer Institute) and cultured in Dulbecco's Modified Eagle Medium (DMEM) supplemented with 10% FBS. SHEP-21N cells were kindly provided by Dr. William Weiss (University of California, San Francisco) and cultured in RPMI supplemented with 10% Tetracycline-Free FBS (Clontech). SHEP-TetOn_MYCN cells were lentivirally engineered (the parental SHEP line was kindly provided by Dr. William Weiss) and cultured in identical conditions to the SHEP-21N cells. BE(2)-C_shTWIST1,2 cells were lentiviral engineered and cultured in DMEM supplemented with 10% Tetracycline-Free FBS. Controllable expression in each respective system was performed by addition of doxycycline (0.2 - 0.5 μg/mL) to growth media. The Multiple myeloma cell lines MM.1S and U266 were purchased from American Type Culture Collection (ATCC) and cultured in RPMI supplemented with 10% FBS. All cell lines were tested for mycoplasma using the MycoAlert kit (Lonza, LT07-218) following manufacturers instructions.

Cell line engineering.

Lentiviral vector cloning.—A MYCN cDNA was cloned into the Tet-On pLIX401 vector obtained from Addgene (a gift from David Root, Addgene plasmid # 41393) via gateway recombination. All clones were digest confirmed and sequence verified. Inducible shRNA constructs targeting TWIST1 were purchased from Cellecta in the following vector: pRSIT16-U6Tet-sh-CMV-TetRep-2A-TagRFP-2A-Puro. Human TCF3 shRNA vectors were purchased from Dharmacon in the GIPZ lentiviral shRNAmir vector (Clone V2LHS_168969, Clone V2LHS_168972, Clone V2LHS_221776).

Lentiviral production and infection.—Lentiviral particles were produced using 2nd generation packaging plasmids psPAX2 and pMD2.G obtained from Addgene (a gift from Didier Trono, Addgene plasmid #s 1226 and 12259). 293FT cells (ThermoFisher) were cultured in DMEM supplemented with 10% FBS, NEAA, and sodium pyruvate per manufactures instructions and transfected using Lipofectamine 2000 (ThermoFisher,). Viral supernatant was collected 48 and 72 hours after infection, filtered through a 0.45μM filter

(EMD Millipore), and concentrated with Lenti-X concentrator (Clontech). Target cells were transduced with concentrated virus in the presence of 8μg/mL of polybrene via spin-fection (2000 rpm for 1 hour). After 24 hours, cells were re-plated in the presence of 0.5-2μg/mL puromycin for 48-72 hours. SHEP parental cells (kindly provided by Dr. William Weiss, UCSF) were transduced with Tet-On MYCN lentiviral particles to generate the SHEP-TetOn_MYCN cell line. BE(2)-C cells were transduced with each respective inducible shRNA targeting TWIST1 to generate the BE(2)-C_shTWIST cell lines. Multiple myeloma cells (MM.1S and U266) were transduced with shRNAs to targeting TCF3 to generate stable TCF3 knockdowns.

Immunoblotting.

For whole cell lysates, cells were lysed using RIPA buffer supplemented with protease inhibitor cocktail (Roche) for 20 minutes. Lysates were clarified at 16,000 g for 15 minutes at 4°C and protein concentration was determined using BCA assay (Pierce). For cell normalized blots, cell numbers were determined using the Countess automated cell counter (Invitrogen) prior to RIPA lysis. A histone extraction was performed for histone blots on cell normalized pellets by acid extraction. Cells were lysed in Triton Extraction Buffer followed by an overnight acid extraction in 0.2N HCL overnight. Antibodies for western blot were purchased as follows: MYCN (Santa Cruz, sc-56729), Vinculin (Santa cruz, sc-25336), GAPDH (Cell signaling, 2118), H3K27Ac (abcam, ab4729), H3 (Cell Signaling, 3638S), TWIST1 (abcam, ab50887). Blots were imaged using fluorescence-labeled secondary antibodies (LI-COR) on the OdysseyCLX Imager (LI-COR). All western blots are shown as cropped images with full scan blots provided with molecular weight/size markers labeled (Supplementary Figure 11-12).

RNA isolation.

Prior to RNA isolation, cell numbers were determined using the Countess automated cell counter Invitrogen. Total RNA isolation was performed using the miRvana miRNA total RNA isolation kit (ThermoFisher Scientific, AM1560) according to manufacturers instructions. Following isolation, RNA was digested with DNase (Ambion). During isolation, external RNA spike-ins (ERCC, Ambion) were added at the time of cell lysis. Total RNA was subject to polyA selection and adapter ligation in preparation for next-generation sequencing (Illumina stranded mRNA library prep) on Nextseq (75 basepair, single-end).

siRNA transfection.

Neuroblastoma cells were reverse transfected (Lipofectamine RNAiMAX, Invitrogen) with 40 nM individual siRNA duplexes (Dharmacon). Protein knockdown was assessed 48 hours post transfection and viable cell count measurements were made 72 hours post transfection using the Countess automated cell counter (Invitrogen) in biological triplicate.

Quantitative RT-PCR analysis.

Expression of human TCF3 transcript was determined using real-time quantitative reverse transcriptase-polymerase chain reaction (qPCR) based on TaqMan fluorescence

methodology, following manufacturer protocols (Applied Biosystems, Foster City, CA). The GAPDH gene was used as housekeeping control. Relative expression was calculated using the comparative delta delta (Ct) method.

Cell proliferation, viability and apoptosis assay.

MM cell proliferation was measured by (3H)thymidine uptake incorporation assay following manufactures instructions (PerkinElmer, Boston, MA). Cell viability was analyzed by CellTiter Glow (CTG) following manufactures instructions (Promega). Apoptosis was evaluated by flow cytometric analysis following Annexin-V (PE) and DAPI staining.

RNA cell count microarray expression analysis.

Biotinylated RNA was prepared according to the standard Affymetrix protocol from 100 nanograms total RNA. Following fragmentation, 12.5 μg of RNA were hybridized at 45°C for 16 hours at 60 RPM on GeneChip Arrays (PrimeView). GeneChips were washed and stained in the Affymetrix Fluidics Station 450 according to the manufacturers instructions, using the buffers provided in the Affymetrix GeneChip hybridization, wash and stain Kit. GeneChips were scanned using the GeneChip Scanner 3000 and images were extracted with Affymetrix GeneChip Expression Console.

TH-MYCN tumor/tissue harvesting

All experimental protocols were monitored and approved by The Institute of Cancer Research Animal Welfare and Ethical Review Body, in compliance with guidelines specified by the UK Home Office Animals (Scientific Procedures) Act 1986 and the United Kingdom National Cancer Research Institute guidelines for the welfare of animals in cancer research (Workman et al., 2010). TH-*MYCN* mice were genotyped to detect the presence of human *MYCN* transgene [28]. Palpable intra-abdominal tumors or ganglia from TH-*MYCN* mice at 12-14 days of age were dissected and harvested for ChIP and immunohistochemistry. For ChIP, tumors and ganglia were immediately flash frozen in liquid nitrogen and stored at −80°C. For immunohistochemistry, tumor and ganglia tissue were immediately fixed in 4% paraformaldehyde before being processed.

Immunohistochemistry

Paraformaldehyde fixed mouse tumor and ganglia tissue were processed for immunohistochemistry using standard methods. Tissue specimens were subject to heat-induced epitope retrieval using citrate buffer (pH 6). The M.O.M kit (Vector Laboratories) was used to minimize non-specific labeling. Tissues were stained with a MYCN antibody (OP13, Calbiochem) followed by a biotynlated mouse secondary antibody (M.O.M kit). Stained specimens were developed using ImmunoPACT substrate (Vector Laboratories) and counterstained with Haematoxylin. After counterstaining, specimens were dehydrated, cleared, and mounted using DPX mountant.

Neuroblastoma patient survival analysis

Matched patient outcome and expression data were obtained for 425 patients from Oberthuer et al., 2010[64]. To link expression of various gene sets overall survival, we first identified

genes with expression data present in the Oberthuer dataset. Across samples, expression values were rank transformed and the median rank of the gene set was used to stratify patients into a high (top 5th percentile) and low (bottom 5th percentile) cohorts. Kaplan-Meyer curves were generated using the R package survival and a KM plotting script authored by Abhijit Dasgupta (see URL section). The statistical significance of the difference between KM curves was tested using a chi-squared test with p-values reported. This analysis was applied for 4 gene sets: top 1,000 genes ranked by total (enhancer + promoter) MYCN load (Fig. 2i), top 1,000 genes ranked by either promoter dominance or enhancer dominance (Supplementary Fig. 7i,j), and top TWIST1 + MYCN occupied genes (Fig. 4h). Analysis was applied to either all neuroblastoma patients (n of 22 in each high/low cohort) or to patients specifically without MYCN genomic amplification (19 in each high/low cohort).

Chromatin immunoprecipitation (ChIP).

Antibodies for ChIP.—Antibodies for ChIP were purchased as follows: MYCN (abcam, ab16898), TWIST1 (abcam, ab50887), H3K27Ac (abcam, ab4729), BRD4 (Bethyl, A301-985A), H3K4me3 (EMD Millipore, 07-473), CTCF (EMD Millipore, 07-729), RNA Pol II (Santa cruz, sc-899).

ChIP.—Chromatin immunoprecipitations were performed as described with minor changes[65]. Neuroblastoma cell lines were grown to 75% confluence in 15 cm plates and cross-linked with 1% formaldehyde (10 minutes) followed by quenching (125 mM glycine). Cells were washed in cold PBS and harvested by cell scraper in cold PBS with protease inhibitors (Roche). Cells were centrifuged at 1650 x g for 5 minutes and flash frozen and stored at −80°C 50E06 cells per pellet. Pellets were resuspended in cytosolic then nuclear lysis buffer and DNA was sheared at 4°C using a waterbath sonicator (Bioruptor, Diagenode) for 25 minutes at high output (30” on, 30” off) in 1mL of sonication buffer supplemented with 0.5% SDS. Sonicated lysates were cleared by centrifuging at 20,000g for 10 min and incubated overnight end-over-end at 4°C with magnetic beads prebound with antibody. Beads were washed three times with sonication buffer, one time with sonication buffer with 500 mM NaCl added, one time with LiCl wash buffer (20 mM Tris pH 8.0, 1 mM EDTA, 250mMLiCl, 0.5% NP-40, 0.5% Na-deoxycholate) and once with TE. DNA was eluted in elution buffer (50 mM Tris-HCl pH 8, 10mM EDTA, and 1% SDS). Cross-links were reversed overnight at 65°C. RNA and protein were digested with 0.2mg/mL RNase A for two hours followed by 0.2mg/mL Proteinase K for one hr. DNA was purified with phenol chloroform extraction and ethanol precipitation.

ChIP-Rx.—ChIP-Rx was performed as described previously substituting mouse embryonic stem cells in place of *Drosophila* S2 cells [66]. Mouse embryonic stem (ES) cells were grown to 75% confluence and cross-linked with 1% formaldehyde followed by quenching (125 mM glycine) as described in the previous section. Cells were washed in cold PBS and harvested by cell scraper in cold PBS with protease inhibitors (Roche). Cells were centrifuged at 1650 x g for 5 minutes and flash frozen and stored at −80°C 10E06 cells per pellet. Fixed mouse ES cell pellets were resuspended in a cytosolic lysis buffer and then spiked directly into the cytosolic lysate of fixed neuroblastoma cells at a ratio of 5% of the total number of cells.

The lysate (neuroblastoma cells spiked with mouse ES cells) was then carried through the ChIP protocol.

TH-MYCN tumor/tissue ChIP.—Flash frozen tumor tissue (30-50 mg chunks) and ganglia (pool of 10-15 ganglia per ChIP) were minced in 1% formaldehyde and incubated for 10 minutes followed by quenching (125 mM glycine). Quenched tissue pellets were resuspended in cytosolic lysis buffer and homogenized with a Dounce homogenizer using 10 strokes with pestle A and 10 strokes pestle B. The homogenized pellets were then spun down, resuspended in nuclear lysis buffer and all subsequent steps were carried out as described for ChIP of neuroblastoma cell lines.

Library Preparation.—Libraries for sequencing were prepared using the Rubicon Thruplex DNA-seq/FD library preparation kit. An input of 50 ng of DNA or less were used and following ligation libraries were amplified per manufacturers instructions. Amplified libraries were then size-selected using AMPure beads (Agencourt AMPure XP) per manufacturers instruction. Further size selection was performed using a 2% gel cassette in the Pippin Prep (SAGE Sciences) set to capture fragments between 200 - 700 base pairs. Libraries were multiplexed at equimolar ratios and run together either on a HiSeq2000 (40 base pair, single end) or on a NextSeq (75 base pair, single-end).

Assay for transposase-accessible chromatin (ATAC).

For each cell line, 50,000 cells were lysed for 10 minutes at 4°C in lysis buffer 10 mM Tris-HCl pH 7.4, 10 mM NaCl, 3 mM MgCl2, 0.1% IGEPAL CA-360). After lysis, the pellets were subject to a transposition reaction (37°C, 60 minutes) using the 2X TD buffer and transposase enzyme (Illumina Nextera DNA preparation kit, FC-121-1030). The transposition mixture was purified using a Qiagen MinElute PCR purification kit. Library amplification was performed using custom Nextera primers and the number of total cycles determined by running a SYBR-dye based qPCR reaction and calculating the cycle number that corresponds to ¼ the maximum. Amplified libraries were purified using a Qiagen PCR purification kit and sequenced on a single lane of an Illumina NextSeq.

CRISPR-Cas9 mutagenesis scanning.

Cas9 was stably expressed in the BE(2)-C cell line via lentiviral transduction (a gift from Feng Zhang, Addgene #52962). Cells were selected in 10μg of Blasticidin and expression checked by western blot (Cas9 antibody: EMD Millipore, MAC133).

sgRNAs were designed to target all possible PAM sequences on both the plus and minus strand of the TWIST1 and NSD1 regions as part of a larger library (total of 5,337 guides). Any sgRNAs that were predicted to align to more than one unique region in the genome were excluded. Single stranded oligos were purchased from CustomArray, Inc. in pooled format, PCR amplified, and cloned by Gibson assembly into the U6-sgRNA-EFS-GFP vector (Addgene #65656). The ligation product was transformed into electrocompetent cells and quality of the library was evaluated via Illumina sequencing for proper representation.

For lentiviral packaging, HEK293T cells were transfected with pVSVg, psPAX2, and sgRNA using Lipofectamine 2000 (Invitrogen). Viral supernatants were harvested, filtered and concentrated via Lenti-X Concentrator solution (Clontech, 631232) following manufacturers instructions. Viral titer was calculated by a dilution series with measurements of GFP positivity (Guava Easycyte flow HT, Millipore). We aimed for one sgRNA per cell with a multiplicity of infection (MOI) of approximately 0.3 - 0.4. A total of 24E06 cells were transduced and maintained at all times during the screen to ensure at least 1000x coverage.

The genomic DNA was isolated at day 15 using the Blood and cell culture DNA maxi kit (Qiagen, 13362) following manufacturers instructions. Libraries were constructed as described previously [67]. A set of 60 PCR reactions were carried out to amplify the sgRNA cassette, pooled, and subsequently prepared for Illumina sequencing on a NextSeq 500.

The read counts for each individual sgRNA were calculated at an early time point (day 4) and a late time point (day 15). The log2 fold change of the early over the late time point was calculated.

Supplementary Material

Refer to Web version on PubMed Central for supplementary material.

Acknowledgements

C.Y.L is supported by the Cancer Prevention Research Institute of Texas (RR150093) and by the NCI (1R01CA215452-01). R.Z. and J.E.B. are supported by V Foundation for Cancer Research Translational Grant. We thank Z. Herbert for his expertise and guidance with next generation sequencing. We thank R. Young and D. Hnisz for assistance with reagents. We thank P. Rahl, C. Ott, and J. Perry for helpful comments on the manuscript.

References

1. Beroukhim R et al. The landscape of somatic copy-number alteration across human cancers. Nature 463, 899–1804 (2010). [PubMed: 20164920]
2. Nesbit CE, Tersak JM & Prochownik EV MYC oncogenes and human neoplastic disease. Oncogene 18, 3004–3016 (1999). [PubMed: 10378696]
3. Matthay KK, George RE & Yu AL Promising therapeutic targets in neuroblastoma. Clinical cancer research : an official journal of the American Association for Cancer Research 18, 2740–2753 (2012). [PubMed: 22589483]
4. Seeger RC et al. Association of multiple copies of the N-myc oncogene with rapid progression of neuroblastomas. The New England journal of medicine 313, 1111–1116 (1985). [PubMed: 4047115]
5. William AW, Ken A, Gayatry M, Burt GF & Bishop JM Targeted expression of MYCN causes neuroblastoma in transgenic mice. The EMBO Journal 16, 2985–2995 (1997). [PubMed: 9214616]
6. Wakamatsu Y, Watanabe Y, Nakamura H & Kondoh H Regulation of the neural crest cell fate by N-myc: promotion of ventral migration and neuronal differentiation. Development 124, 1953–1962 (1997). [PubMed: 9169842]
7. Kang JH et al. MYCN silencing induces differentiation and apoptosis in human neuroblastoma cells. Biochemical and biophysical research communications 351, 192–197 (2006). [PubMed: 17055458]
8. Tweddle DA, Malcolm AJ, Cole M, Pearson AD & Lunec J p53 cellular localization and function in neuroblastoma: evidence for defective G(1) arrest despite WAF1 induction in MYCN-amplified cells. The American journal of pathology 158, 2067–2077 (2001). [PubMed: 11395384]

9. Muth D et al. Transcriptional repression of SKP2 is impaired in MYCN-amplified neuroblastoma. Cancer research 70, 3791–3802 (2010). [PubMed: 20424123]
10. Bell E, Lunec J & Tweddle DA Cell cycle regulation targets of MYCN identified by gene expression microarrays. Cell cycle 6, 1249–1256 (2007). [PubMed: 17495526]
11. Yaari S et al. Disruption of cooperation between Ras and MycN in human neuroblastoma cells promotes growth arrest. Clinical cancer research : an official journal of the American Association for Cancer Research 11, 4321–4330 (2005). [PubMed: 15958613]
12. Tonelli R et al. Anti-gene peptide nucleic acid specifically inhibits MYCN expression in human neuroblastoma cells leading to cell growth inhibition and apoptosis. Molecular cancer therapeutics 4, 779–786 (2005). [PubMed: 15897242]
13. Negroni A et al. Decrease of proliferation rate and induction of differentiation by a MYCN antisense DNA oligomer in a human neuroblastoma cell line. Cell growth & differentiation : the molecular biology journal of the American Association for Cancer Research 2, 511–518 (1991). [PubMed: 1751406]
14. Burkhart CA et al. Effects of MYCN antisense oligonucleotide administration on tumorigenesis in a murine model of neuroblastoma. Journal of the National Cancer Institute 95, 1394–1403 (2003). [PubMed: 13130115]
15. William Clay G et al. Drugging MYCN through an Allosteric Transition in Aurora Kinase A. Cancer Cell 26 (2014).
16. Edmond C et al. CDK7 Inhibition Suppresses Super-Enhancer-Linked Oncogenic Transcription in MYCN-Driven Cancer. Cell 159 (2014).
17. Puissant A et al. Targeting MYCN in neuroblastoma by BET bromodomain inhibition. Cancer discovery 3, 308–323 (2013). [PubMed: 23430699]
18. Nie Z et al. c-Myc is a universal amplifier of expressed genes in lymphocytes and embryonic stem cells. Cell 151, 68–79 (2012). [PubMed: 23021216]
19. Lin CY et al. Transcriptional Amplification in Tumor Cells with Elevated c-Myc. Cell 151, 56–67 (2012). [PubMed: 23021215]
20. Walz S et al. Activation and repression by oncogenic MYC shape tumour-specific gene expression profiles. Nature 511, 483–487 (2014). [PubMed: 25043018]
21. Sabo A et al. Selective transcriptional regulation by Myc in cellular growth control and lymphomagenesis. Nature 511, 488–492 (2014). [PubMed: 25043028]
22. Guccione E et al. Myc-binding-site recognition in the human genome is determined by chromatin context. Nature cell biology 8, 764–770 (2006). [PubMed: 16767079]
23. Wolf E, Lin CY, Eilers M & Levens DL Taming of the beast: shaping Myc-dependent amplification. Trends in cell biology 25, 241–248 (2015). [PubMed: 25475704]
24. Lutz W et al. Conditional expression of N-myc in human neuroblastoma cells increases expression of alpha-prothymosin and ornithine decarboxylase and accelerates progression into S-phase early after mitogenic stimulation of quiescent cells. Oncogene 13, 803–812 (1996). [PubMed: 8761302]
25. Lorenzin F et al. Different promoter affinities account for specificity in MYC-dependent gene regulation. eLife 5 (2016).
26. Orlando DA et al. Quantitative ChIP-Seq normalization reveals global modulation of the epigenome. Cell reports 9, 1163–1170 (2014). [PubMed: 25437568]
27. Kieffer-Kwon KR et al. Myc Regulates Chromatin Decompaction and Nuclear Architecture during B Cell Activation. Molecular cell (2017).
28. Weiss WA, Aldape K, Mohapatra G, Feuerstein BG & Bishop JM Targeted expression of MYCN causes neuroblastoma in transgenic mice. EMBO J 16, 2985–2995 (1997). [PubMed: 9214616]
29. Powers JT et al. Multiple mechanisms disrupt the let-7 microRNA family in neuroblastoma. Nature 535, 246–251 (2016). [PubMed: 27383785]
30. Modak S & Cheung NK Neuroblastoma: Therapeutic strategies for a clinical enigma. Cancer treatment reviews 36, 307–317 (2010). [PubMed: 20227189]
31. Maniatis T, Goodbourn S & Fischer JA Regulation of inducible and tissue-specific gene expression. Science 236, 1237–1245 (1987). [PubMed: 3296191]

32. Visel A et al. ChIP-seq accurately predicts tissue-specific activity of enhancers. Nature 457, 854–858 (2009). [PubMed: 19212405]
33. Shaffer AL et al. IRF4 addiction in multiple myeloma. Nature 454, 226–231 (2008). [PubMed: 18568025]
34. Dang CV et al. The c-Myc target gene network. Elsevier 16, 253–264 (2006).
35. Ji H et al. Cell-type independent MYC target genes reveal a primordial signature involved in biomass accumulation. PloS one (2011).
36. Kim YH, Girard L, Giacomini CP & Wang P Combined microarray analysis of small cell lung cancer reveals altered apoptotic balance and distinct expression signatures of MYC family gene amplification. Oncogene (2006).
37. Schlosser I, Hölzel M, Hoffmann R & Burtscher H Dissection of transcriptional programmes in response to serum and c-Myc in a human B-cell line. Oncogene (2005).
38. Schuhmacher M, Kohlhuber F & Hölzel M The transcriptional program of a human B cell line in response to Myc. Nucleic acids … (2001).
39. Zeller KI, Jegga AG, Aronow BJ & O'Donnell KA An integrated database of genes responsive to the Myc oncogenic transcription factor: identification of direct genomic targets. Genome … (2003).
40. Matthay KK et al. Treatment of high-risk neuroblastoma with intensive chemotherapy, radiotherapy, autologous bone marrow transplantation, and 13-cis-retinoic acid. Children's Cancer Group. The New England journal of medicine 341, 1165–1173 (1999).
41. Wong MP et al. Chromosomal aberrations of primary lung adenocarcinomas in nonsmokers. Cancer 97, 1263–1270 (2003). [PubMed: 12599234]
42. Aggarwal R, Ghobrial IM & Roodman GD Chemokines in multiple myeloma. Experimental hematology 34, 1289–1295 (2006). [PubMed: 16982321]
43. Pellat-Deceunynck C et al. Expression of CD28 and CD40 in human myeloma cells: a comparative study with normal plasma cells. Blood 84, 2597–2603 (1994). [PubMed: 7522634]
44. Tong AW et al. CD40 ligand-induced apoptosis is Fas-independent in human multiple myeloma cells. Leukemia & lymphoma 36, 543–558 (2000). [PubMed: 10784400]
45. Westendorf JJ et al. CD40 expression in malignant plasma cells. Role in stimulation of autocrine IL-6 secretion by a human myeloma cell line. Journal of immunology (Baltimore, Md. : 1950) 152, 117–128 (1994).
46. Staege MS et al. MYC overexpression imposes a nonimmunogenic phenotype on Epstein-Barr virus-infected B cells. Proceedings of the National Academy of Sciences of the United States of America 99, 4550–4555 (2002). [PubMed: 11917131]
47. Masui K et al. mTOR complex 2 controls glycolytic metabolism in glioblastoma through FoxO acetylation and upregulation of c-Myc. Cell Metab 18, 726–739 (2013). [PubMed: 24140020]
48. Suva ML et al. EZH2 is essential for glioblastoma cancer stem cell maintenance. Cancer research 69, 9211–9218 (2009). [PubMed: 19934320]
49. Wang C et al. EZH2 Mediates epigenetic silencing of neuroblastoma suppressor genes CASZ1, CLU, RUNX3, and NGFR. Cancer research 72, 315–324 (2012). [PubMed: 22068036]
50. Hnisz D et al. Super-enhancers in the control of cell identity and disease. Cell 155, 934–947 (2013). [PubMed: 24119843]
51. Whyte WA et al. Master transcription factors and mediator establish super-enhancers at key cell identity genes. Cell 153, 307–319 (2013). [PubMed: 23582322]
52. Lin CY et al. Active medulloblastoma enhancers reveal subgroup-specific cellular origins. Nature (2016).
53. Saint-André V et al. Models of human core transcriptional regulatory circuitries. Genome research (2016).
54. Geerts D, Schilderink N, Jorritsma G & Versteeg R The role of the MEIS homeobox genes in neuroblastoma. Cancer letters 197, 87–92 (2003). [PubMed: 12880965]
55. Dowen JM et al. Control of cell identity genes occurs in insulated neighborhoods in mammalian chromosomes. Cell 159, 374–387 (2014). [PubMed: 25303531]

56. Reiff T et al. Neuroblastoma phox2b variants stimulate proliferation and dedifferentiation of immature sympathetic neurons. The Journal of neuroscience : the official journal of the Society for Neuroscience 30, 905–915 (2010). [PubMed: 20089899]
57. Boeva V et al. Heterogeneity of neuroblastoma cell identity defined by transcriptional circuitries. Nature genetics 49, 1408–1413 (2017). [PubMed: 28740262]
58. van Groningen T et al. Neuroblastoma is composed of two super-enhancer-associated differentiation states. Nature genetics 49, 1261–1266 (2017). [PubMed: 28650485]
59. Entz-Werlé N & Stoetzel C Frequent genomic abnormalities at TWIST in human pediatric osteosarcomas. journal of cancer (2005).
60. Kwok WK, Ling MT, Lee TW, Lau TCM & Zhou C Up-regulation of TWIST in prostate cancer and its implication as a therapeutic target. Cancer research (2005).
61. Kyo S, Sakaguchi J, Ohno S, Mizumoto Y & Maida Y High Twist expression is involved in infiltrative endometrial cancer and affects patient survival. Human pathology (2006).
62. Valsesia-Wittmann S et al. Oncogenic cooperation between H-Twist and N-Myc overrides failsafe programs in cancer cells. Cancer cell 6, 625–630 (2004). [PubMed: 15607966]
63. Littlewood TD, Kreuzaler P & Evan GI All things to all people. Cell 151, 11–13 (2012). [PubMed: 23021211]
64. Oberthuer A et al. Comparison of performance of one-color and two-color gene-expression analyses in predicting clinical endpoints of neuroblastoma patients. Pharmacogenomics J 10, 258–266 (2010). [PubMed: 20676065]
65. Chapuy B et al. Discovery and characterization of super-enhancer-associated dependencies in diffuse large B cell lymphoma. Cancer cell 24, 777–790 (2013). [PubMed: 24332044]
66. Orlando DA et al. Quantitative ChIP-Seq Normalization Reveals Global Modulation of the Epigenome. Cell reports 9 (2014).
67. Shalem O et al. Genome-scale CRISPR-Cas9 knockout screening in human cells. Science 343, 84–87 (2014). [PubMed: 24336571]

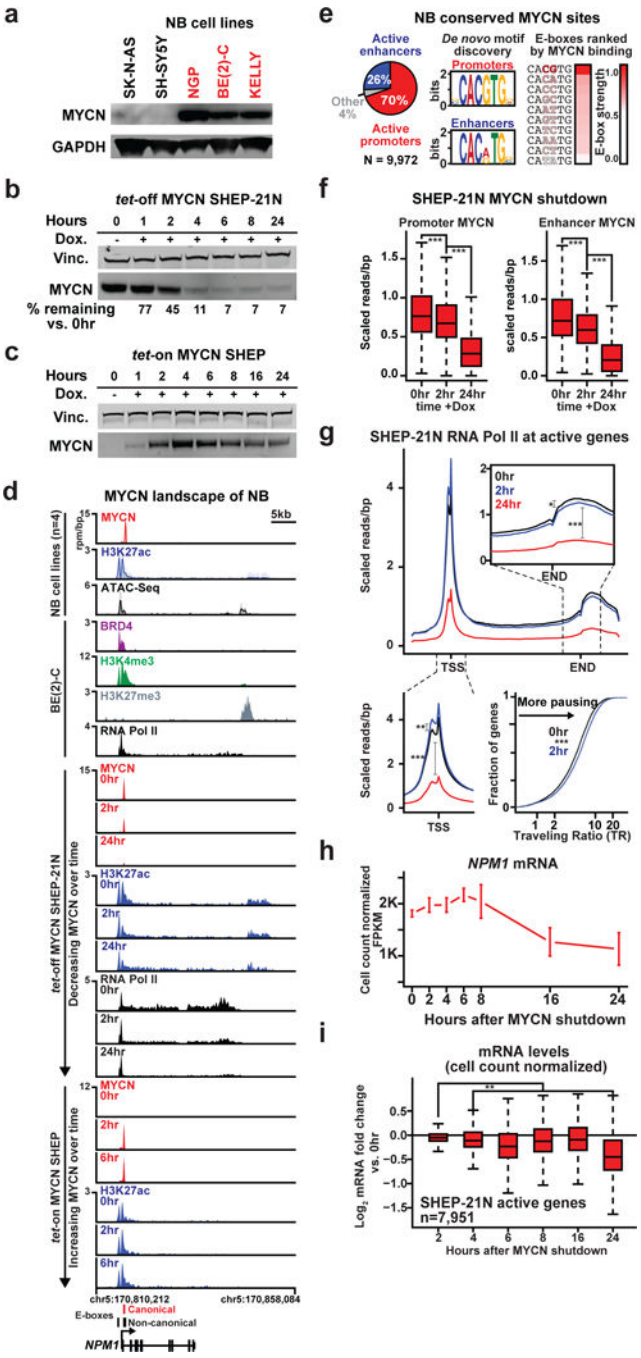

Figure 1: Deregulated MYCN binds active chromatin and amplifies transcription in neuroblastoma

Cropped western blot of MYCN protein levels in human neuroblastoma cell lines., a. Cropped western blot of MYCN protein levels upon MYCN shutdown in the SHEP21-N cell line. The percent of MYCN remaining versus 0hr is indicated and calculated based on pixel intensity quantification., b. Cropped western blot of MYCN protein levels upon MYCN expression in the *tet*-on engineered SHEP cell line. c. ChIP-seq signal (rpm/bp) of the indicated marks at the *NPM1* locus across a panel of neuroblastoma cell line models (MYCN amplified cell lines and inducible MYCN systems). Meta track representation

across four neuroblastoma cell lines shown for MYCN and H3K27ac (top). , d. (Left) Pie chart showing the genomic distribution of conserved MYCN binding regions across four neuroblastoma cell lines. (Middle) *De novo* motif analysis of conserved MYCN binding regions across four neuroblastoma lines. (Right) Heat map of conserved MYCN binding occupancy at E-box sequences. , e. Box plots of MYCN ChIP-seq signal at promoters (left) and enhancers (right) upon MYCN shutdown. Significant differences at 0, 2, and 24hrs denoted; Welch's two tailed *t*-test: *** p-value < 1e-9. **p-value <1e-6., f. RNA Pol II meta gene across all active genes upon MYCN shutdown. The TSS and gene body is magnified and significance denoted. (Bottom right) Distribution plots of RNA Pol II TR for all active genes. Differences in the TR distribution at 0hr and 2hr are significant; Welch's two tailed *t*-test: *** p-value < 1e-9. **p-value <1e-6., g. mRNA levels of the *NPM1* transcript during MYCN shutdown. Units are cell count normalized fpkm for triplicate biological replicates. Error bars represent standard deviation (s.d.)., h. Box plots of $\log_2$ fold changes in active gene expression at the indicated time points versus 0hr post MYCN shutdown. Differences between 2 vs. 8hrs and 4 vs. 24hrs are significant; Welch's two tailed *t*-test: *** p-value < 1e-9. **p-value <1e-6.

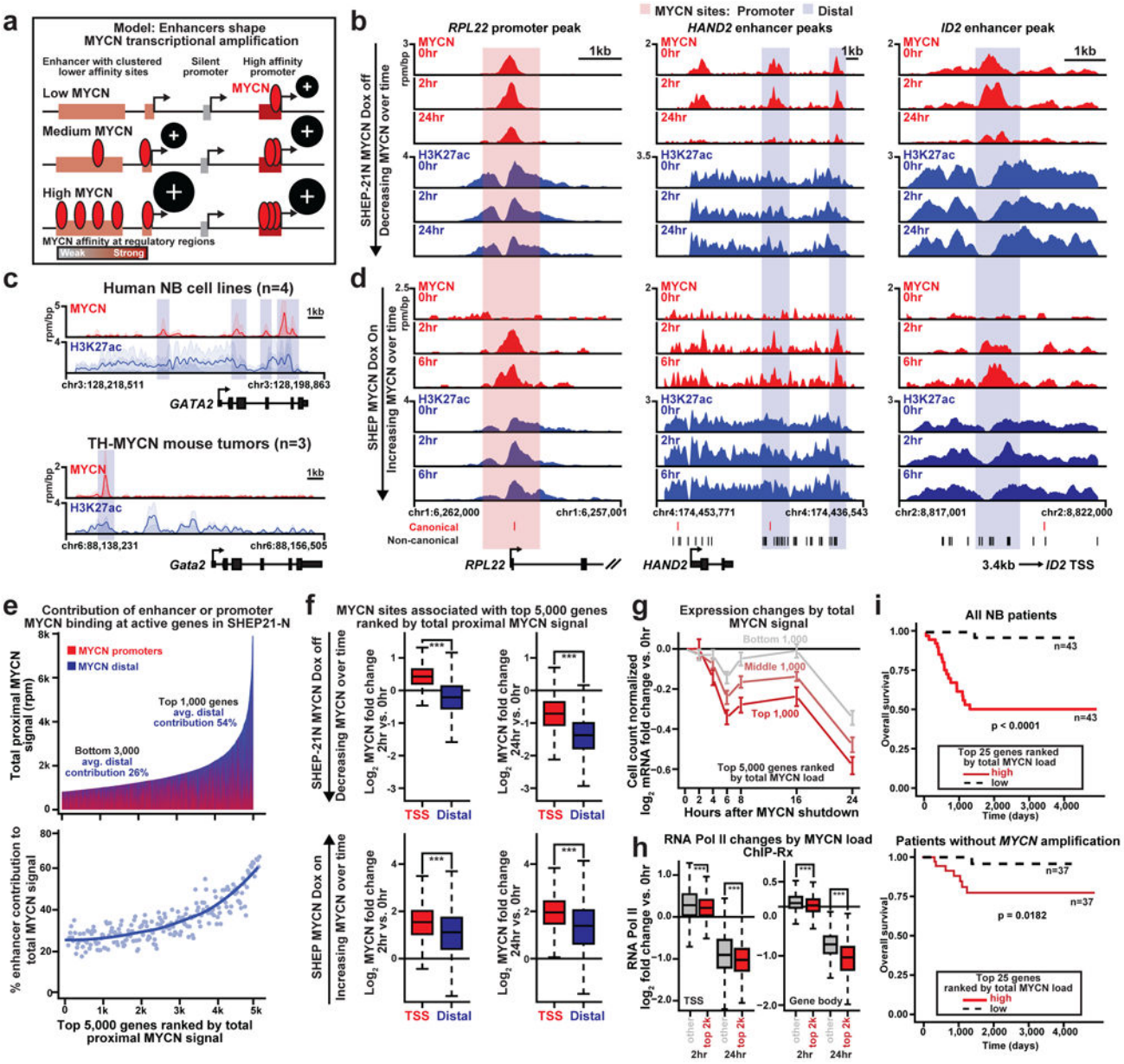

Figure 2: Enhancer invasion shapes MYCN transcriptional response in neuroblastoma

a. Schematic illustrating a model in which clusters of low affinity E-boxes at enhancers shape deregulated MYCN transcriptional amplification b. ChIP-seq tracks of MYCN and H3K27ac at 0, 2 and 24hrs post MYCN shutdown at *RPL22*, *HAND2* and the upstream *ID2* enhancer. c. Meta track representation of MYCN and H3K27ac ChIP-seq signal (rpm/bp) across (top) four neuroblastoma cell lines and (bottom) and three TH-MYCN tumors at the *GATA2* locus. d. ChIP-seq tracks of MYCN and H3K27ac at 0, 2 and 6hrs post MYCN induction at *RPL22*, *HAND2* and the upstream *ID2* enhancer. e. (Top) Plot showing the top 5,000 genes (x-axis) in SHEP21 ranked by total proximal MYCN signal (y-axis). (Bottom) Dot plot of % enhancer contribution (enhancer/total MYCN signal) sampled across bins (100 genes/bin) with a best fit line superimposed (loess correlation).f. Box plots of the $\log_2$

fold change of MYCN load at the TSS and distal enhancers of the top 5,000 genes ranked by proximal MYCN signal. (Top) $\log_2$ fold change at 2hr and 24hr (versus 0hr) post MYCN shutdown. (Bottom) $\log_2$ fold change at 2 and 6hr (versus 0hr) post MYCN induction. g. Cell count normalized $\log_2$ fold change (versus 0hr) of gene expression changes during MYCN shutdown in the SHEP-21N system. Genes are grouped according to rank ordered MYCN proximal load (promoters and enhancers). Error bars represent 95% confidence interval (CI) of the mean.h. Box plots of the $\log_2$ fold change (versus 0hr) of the amount of RNA Pol II (ChIP-Rx) at the TSS (left) and gene body (right) of genes grouped according to rank ordered MYCN proximal load. Significance is denoted by Welch's two tailed *t*-test: *** p-value < 1e-9. **p-value <1e-6. *p-value <1e-3. i. Overall survival of patients ranked by expression (high or low) of the top 25 genes defined by total MYCN load for all neuroblastoma patients (top) and patients without MYCN amplification (bottom). Significance is denoted by a chi-squared test and p-values are shown.

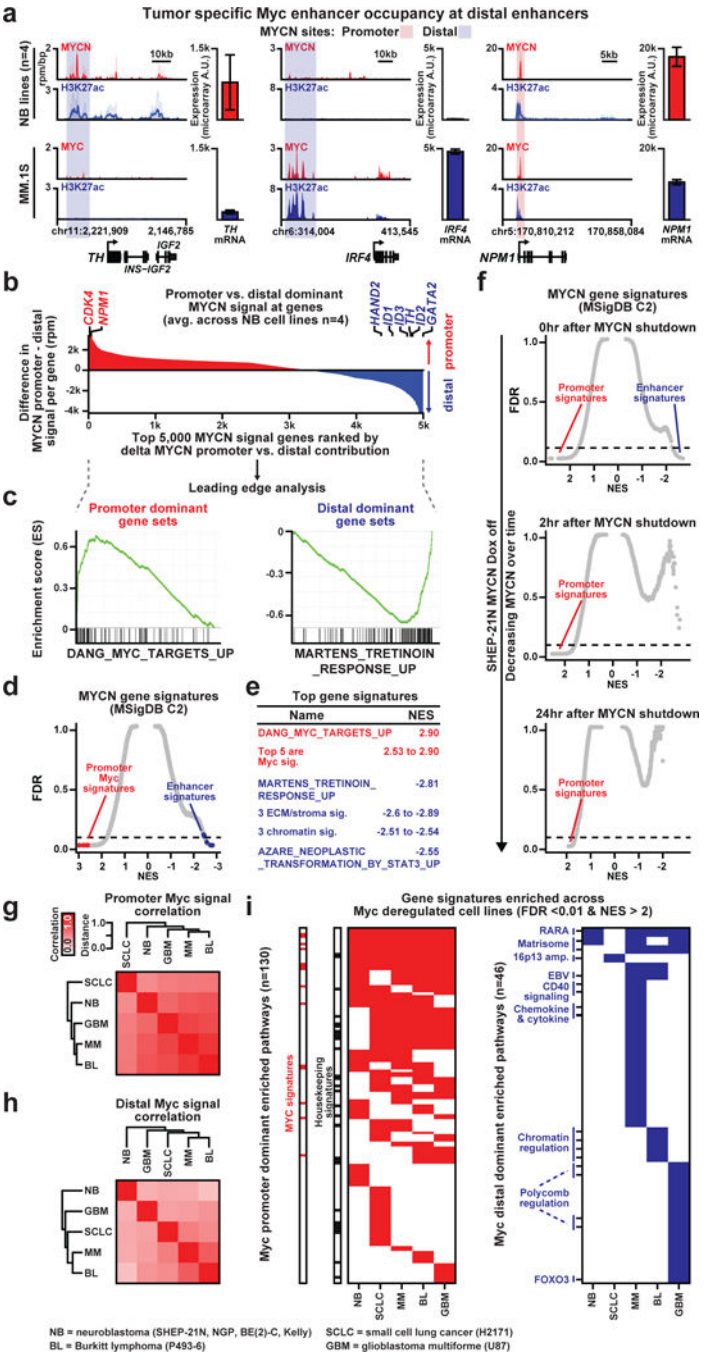

Figure 3: Enhancer invasion accounts for tumor specific MYC/MYCN signatures

a. (Top) Meta track representation of MYCN and H3K27ac ChIP-seg signal (rpm/bp) across four neuroblastoma cell lines at the indicated loci. (Bottom) ChIP-seq tracks of MYC and H3K27ac signal in the MM.1S cell line. mRNA expression levels are shown as a bar plot in each with expression in arbitrary units (A.U.). b. Differential MYCN signal contribution across NB lines for promoters (red) and enhancers (blue) of associated genes (y-axis) of the top 5,000 proximal MYCN bound regions are shown ranked by difference in MYCN enhancer to promoter contribution (x-axis). c. GSEA plots of MYCN bound promoter (red)

versus enhancer (blue) dominant gene sets defined by leading edge analysis. d. Normalized enrichment score (NES) of target gene signatures (Molecular Signature Database) are plotted on the x-axis versus the FDR (false discovery rate) on the y-axis. e. Highly significant gene signatures from promoter (red) and enhancer (blue) bias gene sets are highlighted and tabulated.f. Normalized enrichment score (NES) of target gene signatures (Molecular Signature Database) are plotted on the x-axis versus the FDR (false discovery rate) on the y-axis at 0, 2 and 24hrs post MYCN shutdown. g. Clustering of MYC/MYCN ChIP-seq signal at promoters across MYC/MYCN deregulated cell lines.h. Clustering of MYC/MYCN ChIP-seq signal at enhancers across MYC/MYCN deregulated cell lines.i. Heat-map of gene signatures enriched across MYC/MYCN deregulated cell lines. Selected signatures are annotated at a FDR <0.01 & NES > 2 cutoff.

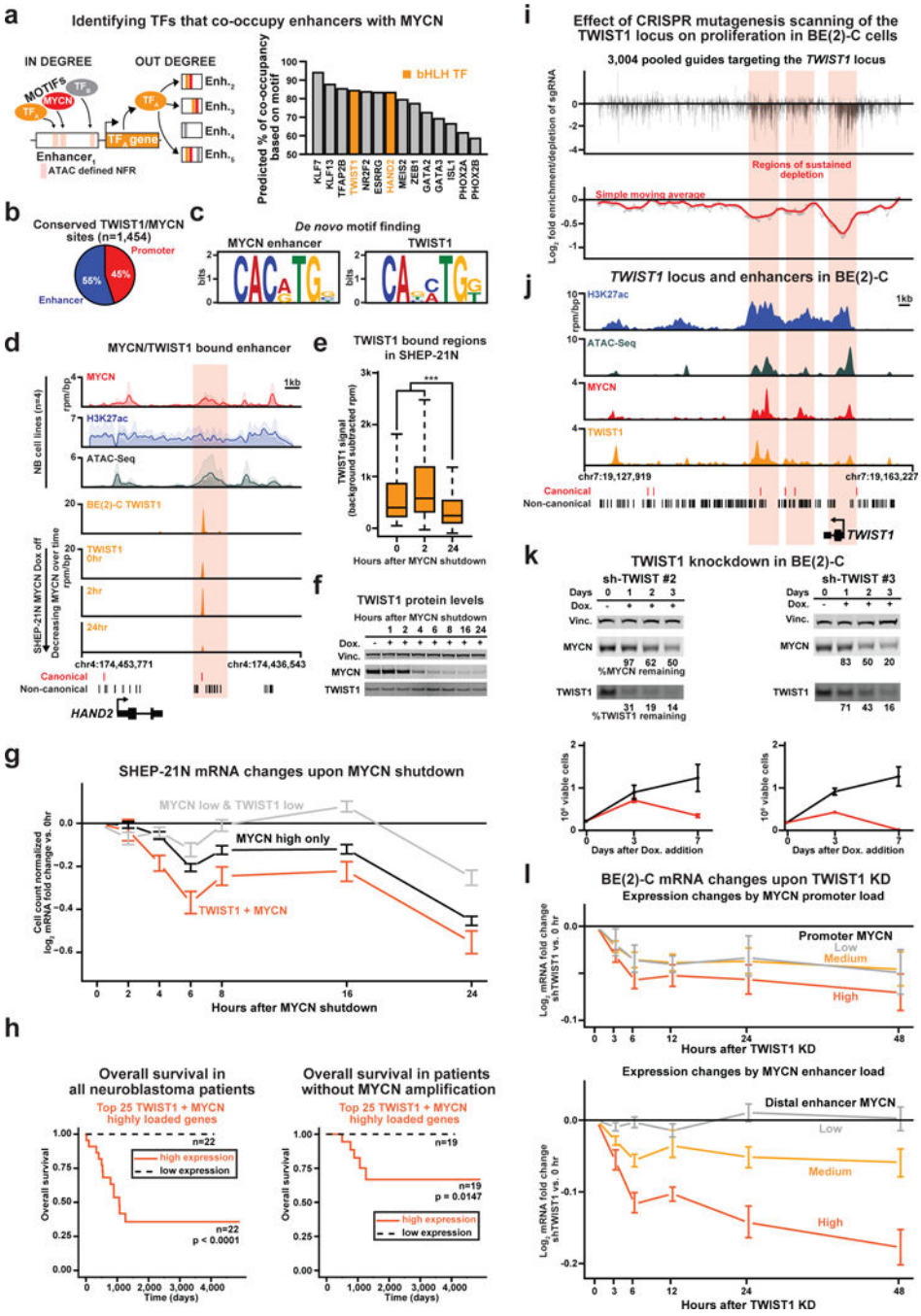

Figure 4: TWIST1 co-occupies enhancers with MYCN and is required for expression of the MYCN enhancer axis

a. (Left) Schematic of the computational approach to identifying a core regulatory circuit based on TF enhancer binding. (Right) Histogram plot ranking core regulatory circuit TFs based on motif co-occupancy with MYCN. b. Pie chart showing the genomic distribution of overlapping TWIST1 and MYCN bound sites. *c. De novo* motif analysis of enhancer regions for MYCN and TWIST1 binding sites. d. Meta track representation of MYCN ChIP-seq signal, H3K27ac ChIP-seq signal, and ATAC-seq signal (rpm/bp) at the *HAND2* locus. Corresponding ChIP-seq signal of TWIST1 in the BE(2)-C and SHEP-21N cell lines during

MYCN shutdown is shown. e. Boxplots of TWIST1 signal at 0, 2 and 24hrs post MYCN shutdown. Significance is denoted, Welch's two tailed *t*-test: *** p-value < 1e-9f. Cropped western blot of Vinculin, MYCN, and TWIST1 levels upon MYCN shut down. g. Cell count normalized $\log_2$ fold change (versus 0hr) of gene expression changes during MYCN shutdown in the SHEP-21N system. Genes are grouped by MYCN and/or TWIST1 binding: MYCN and TWIST1 co-bound sites (yellow), MYCN highly bound sites alone (black) and MYCN and TWIST1 lowly co-bound sites (gray). Error bars represent 95% CI.h. Overall survival of patients ranked by expression (high or low) of genes highly loaded with MYCN and TWIST1 in all neuroblastoma patients (left) and patients without MYCN amplification (right). Significance is denoted by a chi-squared test and p-values are shown.i. CRISPR scan of the TWIST1 locus and its downstream enhancers. (Top) Illumina sequencing readout of $\log_2$ fold enrichment/depletion (early versus late time point) of 3,351 sgRNAs. (Bottom) Simple moving average of $\log_2$ fold enrichment/depletion is shown. j. ChIP-seq signal of H3K27ac (blue), ATAC-seq (green), MYCN (red), and TWIST1 (yellow) at the TWIST1 locus and enhancers with respect to CRISPR sgRNAs. Red shaded boxes highlight regions of marked $\log_2$ fold depletion. k. (Top) Cropped western blots of Vinculin, MYCN, and TWIST1 levels upon TWIST1 knockdown. (Bottom) Viable cell counts at 3 and 7 days post inducible TWIST1 knockdown. l. Log_2 fold change (versus 0hr) of gene expression changes upon TWIST1 knockdown of genes ranked by MYCN promoter load (top) or MYCN distal enhancer load (bottom). Error bars represent 95% CI.